J Mater Sci (2006) 41:5053–5060
DOI 10.1007/s10853-006-0448-2

The effect of the composition of the intergranular film in alumina on preferential adsorption and growth

Stephen H. Garofalini · Shenghong Zhang

Received: 1 December 2005 / Accepted: 16 February 2006 / Published online: 18 July 2006

Abstract Composition of the intergranular film (IGF) found between alumina crystals has been shown to affect growth. Here, we employ molecular dynamics (MD) computer simulations to study the effect of the composition of calcium alumino-silicate IGFs on preferential adsorption and grain growth in α-Al_2O_3 at an atomistic level. The IGF is formed while in contact with two differently oriented crystals, with results showing preferential adsorption and growth along the $[11\bar{2}0]$ direction of the $(11\bar{2}0)$ surface in comparison to that along the surface normal on the (0001) surface for certain calcium alumino-silicate compositions. Such preferential growth is consistent with experimentally observed anisotropic grain growth in alumina, where platelets form because of faster outward growth of the prism orientations than the basal orientation. The simulations show the mechanism by which Ca ions in the IGF inhibit growth on the basal surface and the important role that the Ca/Al ratio in the IGF plays in the change from isotropic to anisotropic grain growth. At compositions with high or low Ca/Al ratios, growth along each surface normal is equivalent, indicating isotropic grain growth. The simulations provide an atomistic view of attachment onto crystal surfaces, affecting grain growth in alumina, and the importance of local chemistry of the IGF on local adsorption and growth behavior.

S. H. Garofalini (✉) · S. Zhang
Interfacial Molecular Science Laboratory, Dept of Materials Science and Engineering, Rutgers University, Piscataway, NJ 08855, USA
e-mail: shg@glass.rutgers.edu

Introduction

Amorphous intergranular films often form between crystals in commercial ceramics because of the presence of impurities in the materials or because of the addition of sintering aids [1–8]. While these films make up only a small volume percent of the material, they can significantly affect microstructural and mechanical properties [9–11]. Ultrapure Al_2O_3 sintered in clean conditions usually shows normal grain growth [12, 13], while commercial alumina usually contains sufficient impurities that modify microstructure, via anisotropic grain growth, and resultant properties. This anisotropic growth forms platelet crystals that have large, flat basal surfaces with thin intergranular films [14–17]. Silicon nitride is another well-studied material that shows anisotropic growth. Although silicon nitride requires sintering aids to enable densification during sintering, these aids create silicate IGFs that also affect the microstructure and properties of the nitride [4, 10, 11, 18–20]. In the nitride case, anisotropic grain growth causes formation of whiskers rather than platelets. While various mechanisms have been invoked to describe grain growth, in both the oxide and nitride cases the IGF affects grain growth, with the implication that the composition in the IGF affects adsorption and growth along the surface normal of specific planes.

Experiments showed that small (ppm) levels of either calcia or silica cause abnormal grain growth (AGG) in alumina [21]. Studies of yttria and silica or titania and silica additions to alumina showed the importance of co-doping on affecting AGG [14, 17]. Understanding the atomistic structure of the IGF in the polycrystalline ceramics is experimentally difficult because of the thin and amorphous structures of these

films, although there has been recent success in studies of IGFs in Si_3N_4 using high resolution transmission electron microscopy (HRTEM) and aberration-corrected High-Angle Annular Dark Field-Scanning Transmission Electron Microscopy (HAADF-STEM) [22–25]. In concert with experiment, computational studies have been used to address these films at the atomistic level [26–40].

One of the more important results from high resolution studies of IGFs is that the concentration within the IGF is often clearly different than the bulk average, with excess species sitting in the triple point or pocket [41]. In that paper, they state that the STEM image of the grain boundary (GB) shows ''two neighboring GB films with remarkably different calcium excesses.'' In fact, the two GB films had the same triple point connecting them, thus showing the importance of the actual grain boundaries and not just the bulk composition. Similar observations regarding preferential Ca segregation at two surface grain boundaries have also been shown by others [9]. Therefore, while bulk composition is important, the local composition within the IGF between different grains appears to play a dominant role in behavior and is different from the bulk composition. As will be shown below regarding our simulation results, this difference in local behavior can significantly affect growth locally and should be a part of our understanding of material behavior.

Our previous simulations of amorphous silicate IGFs in contact with alumina crystals and silicon nitride crystals clearly showed ordered structures at the interfaces and density oscillations into the IGF induced by the crystals [27–29, 36, 37, 42]. Recent aberration-corrected HRTEM studies observe such density oscillations [24]. These density oscillations decay within a nanometer of the interface, attaining a glassy structure in the interior of the thicker films. Most importantly, the previous simulations of IGFs between the differently oriented crystals showed anisotropic growth [37, 42]. The term 'growth' in this discussion means adsorption of species from the IGF onto the crystal surface consistent with the crystal orientation and composition such that the crystal lattice extends along the surface normal of the particular plane in contact with the IGF. In a real system, such adsorption of species from the IGF would require the neighboring crystal to move away as the adsorbing crystal extended outward if the separation distance between the crystals were to remain nearly constant. Such a process could involve dissolution of one crystal, diffusion of species across the interface, and adsorption onto the growing crystal, although other mechanisms can be considered [43]. The adsorbing species from the IGF must be replenished if growth is to continue, so a triple point may also act as a source of ions for the growing crystal. In the simulations, the use of constant pressure along the surface normal enables the crystals to move according to the structural changes in the IGF and at the interfaces. However, we do not replenish the IGF in the current simulations, although the use of a variety of compositions provides useful information regarding the effect of changing local composition on adsorption and growth behavior.

Computational procedure

Similar to previous studies [26–28, 42–28, 44, 45], a multibody interatomic potential was used in the simulations and is given as:

$$V = \sum_{i \neq j} V_{ij}^{\mathrm{BMH}} + \sum_{i \neq j \neq k} V_{jik}^{3-\mathrm{body}} \tag{1}$$

where V_{ij}^{BMH} is the pairwise modified Born–Mayer–Huggins (BMH) potential term and $V_{jik}^{3-\mathrm{body}}$ is the three body potential term. The modified BMH potential is defined as

$$V_{ij}^{\mathrm{BMH}} = A_{ij} \exp\left(\frac{-r_{ij}}{\rho_{ij}}\right) + \frac{z_i z_j e^2}{r_{ij}} \xi\left(\frac{r_{ij}}{\beta_{ij}}\right) \tag{2}$$

The first term is the repulsion term in the modified BMH pair potential and represents the short distance core electron overlap; the second term is a screened Coulomb interaction that reduces the nominal charges of the ions based on ξ (which is a complimentary error function). r_{ij} is the separation distance between the ions i and j; z_i and z_j are the formal charge of the ions; β_{ij} is a species-dependent term that reduces the formal charges as a function of distance between the ij pair. The value of the parameters A_{ij}, β_{ij} and ρ_{ij} for each pair type were previously presented [27, 37, 39, 42, 44]. Ion charges for silicon, oxygen, nitrogen, aluminum and calcium ions are +4, −2, −3, +3 and +2, respectively, although the use of the screening term reduces these charges to values more in line with those observed in ab-initio calculations (which also show variations among them).

The 3-body potential accounts for the effect of partial covalency of some of these species by raising the energy on a central ion within a triplet as the angle deviates from an ideal angle. The 3-body potentials

applied to all Si, O, N, and Al ions as central ions i is given as:

$$V_{jik}^{3-\text{body}} = \lambda_{jik} \exp\left(\frac{\gamma_{ij}}{r_{ij} - r_{ij}^0} + \frac{\gamma_{ik}}{r_{ik} - r_{ik}^0}\right) \Omega_{jik} \quad (3)$$

when $r_{ij} < r_{ij}^0$ and $r_{ik} < r_{ik}^0$.
Otherwise,

$$V_{jik}^{3-\text{body}} = 0 \text{ when } r_{ij} > r_{ij}^0 \text{ or } r_{ik} > r_{ik}^0$$

The angular part, Ω_{jik}, is given as

$$\Omega_{jik} = \left(\cos\theta_{jik} - \cos\theta_{jik}^0\right)^2 \quad (4)$$

for the Si/Al/Ca–**O**–Si/Al/Ca and O–**Si**–O structure, while for the O–**Al**–O triplet, it is defined as

$$\Omega_{jik} = \left[\left(\cos\theta_{jik} - \cos\theta_{jik}^0\right) \sin\theta_{jik} \cos\theta_{jik}\right]^2 \quad (5)$$

where the three atoms form angle θ_{jik} with the central atoms as the vertex i in these triplets for both conditions. Since Ca is considered mainly ionic, no 3-body potential centered on Ca as ions i in the jik triplet is used. The parameters used here have been previously presented [28, 37, 39, 42, 44, 46, 47].

The glassy IGFs were made between two dissimilar α-alumina orientations, the (0001) and (11$\bar{2}$0), creating a (0001) oriented crystal)/(IGF)/(11$\bar{2}$0) oriented crystal) system. A schematic drawing of the system is shown in Fig. 1. The simulation procedure is the same as that previously published [38, 42], where it has been discussed in detail.

Briefly, each crystal is aligned such that the appropriate crystal terminating plane would be in contact with the IGF, as shown in Fig. 1. The atoms in the top few layers of the upper crystal, and the bottom layers of the lower crystal are always frozen so that periodic boundaries can be used in all three dimensions. These frozen atoms are never used as central species in the summations above and therefore never see each other. However, the frozen atoms can act as neighbors to the mobile atoms in the summation over pairs and triplets. These frozen sections move en-masse to any imposed pressure.

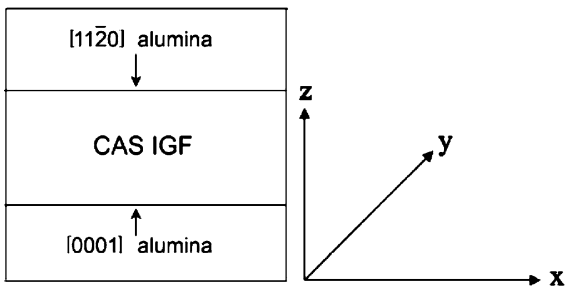

Fig. 1 Schematic view of the IGF/crystal system used in this work. Periodic boundary conditions are used in the X and Y directions

The glassy IGFs are made between the crystals by randomly inserting the atoms of the IGF composition in the volume between the crystals, followed by a melt/quench procedure. Both NVE (constant number, volume, and energy) and NPT (constant number, pressure, and temperature) simulations are used and a timestep of 1×10^{-15}s is used throughout the simulations. The x, y, and z dimensions are approximately 5.2 nm, 5 nm, 10 nm, respectively, and the IGF is ~4 nm thick. IGF thickness in alumina from 1 nm to 5 nm have been reported [14]. We have previously discussed thinner 1–2 nm films [27]. The x and y dimensions change with the thermal expansion coefficient of the crystal to minimize elastic effects. Table 1 gives the nomenclature and the number of atoms in each IGF, as well as the number of species in each alumina crystal. Additional details have been presented elsewhere [42].

Results and discussion

Figure 2 shows the density profiles as a function of the Z coordinate for the atoms in the basal and prism oriented crystals and the sum of the atoms in the IGF for one of the alumina systems. There are density oscillations in the IGF near the interfaces, decaying within ~1 nm from each interface, showing a glassy density profile in the interior of the IGF. Similar density oscillations are observed in the other IGF compositions, as well as in our simulations of the IGF in silicon

Table 1 Composition and system sizes

Sample No.	Mole ratio $CaO:Al_2O_3:SiO_2$	Specific number of atoms				Total
		Ca	Al	Si	O	
112	1:1:2	665	1,330	1,330	5,320	8,645
313	3:1:3	1,296	864	1,296	5,184	8,640
216	2:1:6	640	640	1,920	5,440	8,640
14535	14:5:35	770	550	1,925	5,445	8,690
334	3:3:4	720	1,440	960	4,800	7,920
123	1:2:3	400	1,600	1,200	5,200	8,400
221	2:2:1	1,000	2,000	500	5,000	8,500
121	1:2:1	550	2,200	550	4,950	8,250
141	1:4:1	340	2,720	340	5,100	8,500

The number of atoms in the alumina crystals in the simulation are 7,920 and 8,640 for basal and prism orientations, respectively

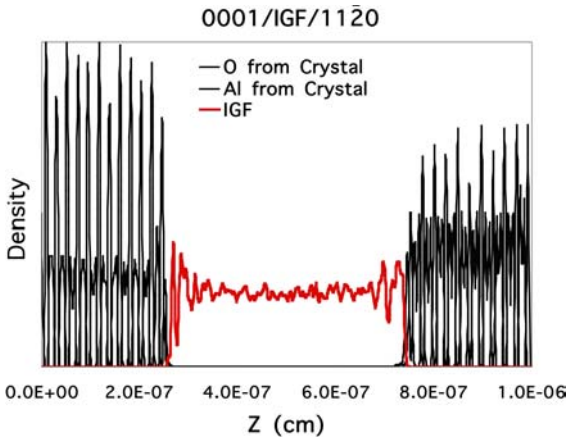

Fig. 2 Density profile of the atoms in the crystals and the sum of the atoms in the IGF as a function of distance in Z, with the basal oriented crystal on the left and the prism oriented crystal on the right. Density oscillations occur in the IGF near the interfaces. A glass-like profile exists in the interior of the IGF

nitride [37, 39], although the thinner dimension (1–2 nm) of the IGF in the nitride means that these density oscillations may impinge on each other. Such density oscillations have been observed in recent aberration-corrected HRTEM [24, 25, 48]. Additional simulations also show that the extent of these oscillations into the IGF would be affected by structural and compositional perturbations in the crystalline surface [49]. Density oscillations could be expected based on data from earlier studies of inert gases in contact with hard walls, but in the current simulations, there is much more chemistry involved in these complex systems than that occurring in simple inert gas systems. The four species present in the IGF (Si, Al, Ca, O) all interact with the two terminated crystal surfaces differently. In order to evaluate these different interactions and their effect on the structure at the interfaces, density profiles of individual species were determined.

Figure 3 shows the density profiles as a function of the Z coordinate for the individual species for the alumina system with the 221(top) and 141 (bottom) calcium alumino-silicate IGF compositions (221 and 141 in Table 1), in which the Al and O are labeled separately in the IGF versus those in the crystals. Growth of a crystal is inferred from the extension of each crystal along its surface normal in each case. This would require adsorption of Al (and O) ions from the IGF onto the specific crystal surface. The basal oriented crystal has crystalline density oscillations of 2 Al peaks, 1 O peak; the prism oriented crystal has crystalline density oscillations of 1 Al peak, 2 O peaks. On the basal side, the crystal terminates with a single layer of Al ions (which has been shown to be the lowest energy configuration [44, 50]), whereas the crystal terminates with a single layer of O on the prism surface. Therefore, extension of the crystals have different required adsorptions from the IGF species: the basal side requires Al to adsorb, creating the second Al layer for extension of the crystal in the surface normal direction, while the prism side requires O adsorption to form the second O layer needed for continuation of the crystal on the prism side, followed by a single Al layer. The arrows in the 221 images indicate the first layer of Al adsorbed from the IGF onto the crystal (or onto O from the IGF that have adsorbed onto the crystal in the prism side). The 141 system shows a much larger first adsorbed Al peak on the basal side, with a splitting of

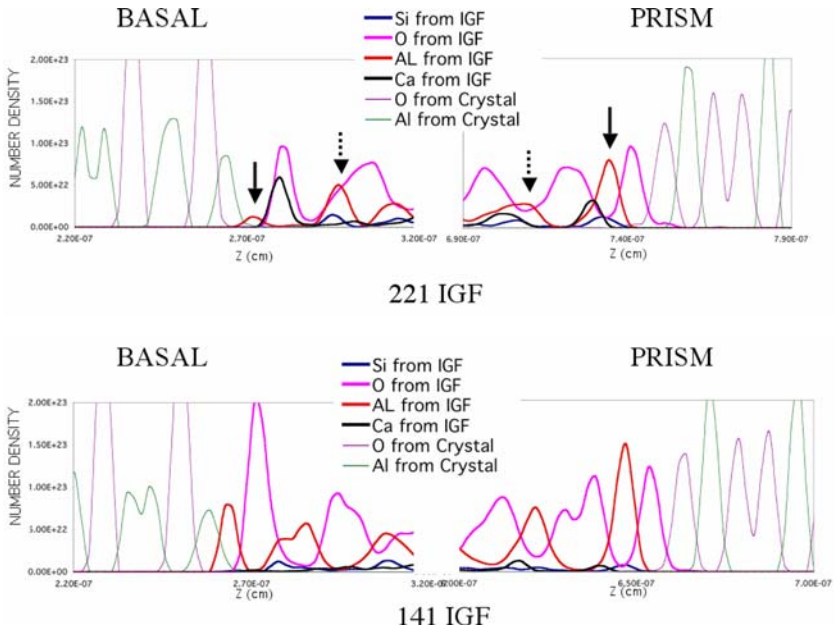

Fig. 3 Expanded view of the density profiles of individual species in the 221 IGF (top) and 141 IGF (bottom) and crystals in the alumina system. The solid arrows in the 221 images point to the first adsorbed Al peak on each side, while the dashed arrow shows the second adsorbed Al peak. Note the splitting of the second Al peak on the basal 141 IGF and the second O peak on the prism 141 IGF profiles; these are indicative of the dual peak nature of these species in the respective crystal orientations

the second adsorbed Al peak (into the dual Al peak, consistent with extension of the crystal with this orientation). Similarly, on the prism side of the 141 system, there is a splitting of the second adsorbed O peak, consistent with the dual nature of the O peaks in the prism oriented crystal.

The first adsorbed Al peak is necessary for growth and can be used to indicate the potential for growth of the specific orientations as a function of composition in the IGF. The area under the first adsorbed Al peak, normalized by the area under the peak of the Al in the crystal for each appropriate crystal orientation, will be used as a measure of the 'growth' of each crystal along its surface normal.

Figure 4 shows the integrated intensity of the normalized first adsorbed Al peak (normalized to the integrated intensity of the crystalline Al peak for the appropriate crystal) for the basal and prism orientations for the alumina case as a function of the Al concentration in the IGF (normalized by the sum of the cations in the IGF). Clearly, adsorption and growth of the alumina is more rapid on the prism surface than on the basal surface over most compositions, indicating anisotropic grain growth. This anisotropy is consistent with experimentally observed anisotropic grain growth in alumina, in which growth along the basal surface normal is slower than that on the prism surface normal. Kwon reported a factor of 5–8 faster growth of the non-basal planes in comparison to the basal plane [14] in alumina with titania–silica codopants in the IGF. The maximum difference in growth in the simulations inferred from the intensities implies a factor of 3.5 for alumina with the CAS IGF. At the highest and lowest Al concentrations, adsorption on the basal surface is similar to that on the prism surface, indicating isotropic grain growth, although the apparent rates would be slow for both surfaces at low Al concentration and much higher for high Al concentration.

The data point at 0.5 Al/all cations (from the 123 system) and the two data points on either side (the 334 and 221) were reproduced in additional simulations with only minor variance, indicating something significant occurring at this specific composition. Considering the effect of the Ca/Al ratio (R) in the IGF on the normalized adsorbed Al peak intensities provides clarification.

One Ca ion charge compensates 2 Al in the tetrahedral sites in the glassy silicate structure. This means that the equivalence point in the glassy structure would have an R value of 0.5. Ca in excess of this equivalence point would create non-bridging oxygen in the silicate glass structure. Similarly, Al in excess of the equivalence point would mean that the glass structure would have to change in a manner previously discussed in detail [51]. Either condition puts the glass structure into a less energetically favorable condition.

Analysis of adsorption behavior as a function of the Ca/Al ratio in the IGF gives a more accurate view of the trends in composition affecting adsorption and growth and is shown in Fig. 5. Here, the normalized integrated intensities of the first adsorbed Al peak are plotted versus the Ca/Al ratios of the IGFs. While there is some spread in the intensity data at any Ca/Al ratio, the trends are quite obvious. At high and low Ca/Al ratios in the IGF, adsorption and growth are similar on both types of orientations, which may be indicative of isotropic growth. Near the Ca/Al ratio equal to 0.5, there is a clear separation of peak intensities and

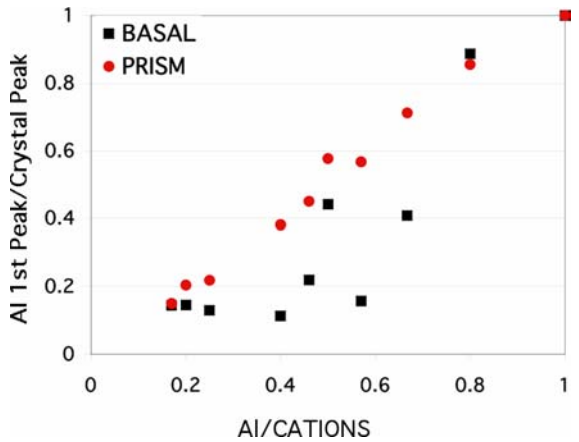

Fig. 4 Normalized area under the first adsorbed Al peak from the IGF onto the different crystal surfaces as a function of the ratio of Al/all cations. Note the significantly faster growth along the prism surface normal than the basal surface normal for most compositions between 0.25 and 0.7

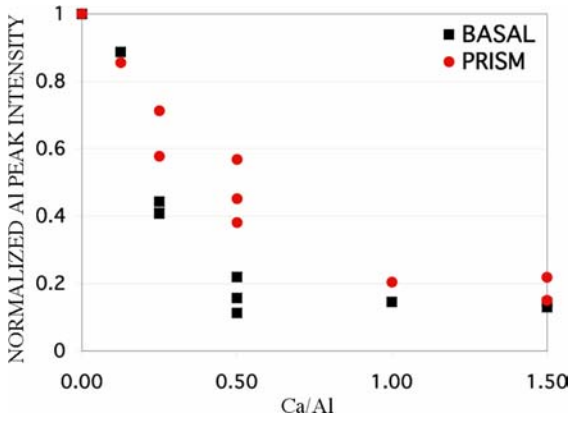

Fig. 5 Normalized area under the first adsorbed Al peak from the IGF onto the different crystal surfaces as a function of the Ca/Al ratio (R). The equivalence point, R_e, is at 0.5. Below R_e, excess Al in the IGF allows for more rapid adsorption of Al onto the basal surface than that above the equivalence point

adsorption behavior onto the two surfaces, which is indicative of anisotropic growth. Again, because of the need to charge compensate Al ions in the silicate glass structure using Ca ions, there is a competition between Al plus associated Ca within the silicate glass, creating a silicate with no non-bridging oxygen, versus Al adsorbing onto the crystal and excess Ca remaining in the glass, forming non-bridging oxygen.

This could also be viewed conversely, in which Al additions to silicate glasses containing network modifiers such as alkali or alkaline earth ions are known to enhance the properties of the glass, such as corrosion resistance, because the Al additions remove the non-bridging oxygen that weaken the silicate network structure. Al addition in excess of associated modifier content in silicates make glass formation difficult because of an increased ease in devitrification [52]. The local structure around the Al ions changes with Al in excess of the modifier content, creating an energetically less favorable condition [51]. In the IGF, excess Al concentrations (R values below 0.5) would similarly have Al ions in less energetically favorable sites in the glass. These would be expected to adsorb onto either crystal surface, with remaining Ca ions charge compensating the Al ions remaining in the IGF. As the Al concentration in the IGF is depleted by this adsorption process, there would be a lowering of the driving force for adsorption onto the crystal surfaces, with adsorption onto the basal surface decreasing first. With a source of ions from a triple point, which could be similarly replenished by nearby dissolving crystals at high processing temperatures, depletion could be offset, but that is not the case in the current simulations.

At low Ca/Al ratios, Al in the IGF is in excess of Ca and therefore readily adsorb onto either surface. At the high Ca/Al ratios used here, Al adsorption onto either crystal surface is much lower.

The different adsorption and growth behavior on the different surfaces is caused by the presence of Ca in the IGF and the Ca/Al ratio. The concentration of Si may be expected to play an important role in the extremes of compositions [9], but not in the systems we studied here. Figure 6 shows a snapshot of a side view of the basal oriented crystal that has an anorthite composition. The figure clearly shows the 'cage' structure formed at the interface with the IGF. Ca ions preferentially adsorb into the cage interiors, inhibiting Al adsorption onto the crystal sites that would otherwise continue the crystal structure in this orientation. With excess Ca in the IGF and the presence of available surface sites at the crystal surfaces, Ca ions segregate to the interface to charge compensate undercoordinated O at the crystal surface, as well as the zeolitic oxygen in the Al-O-Si sites at the 'cage' sides. As will be shown in Fig. 7, with sufficiently high concentrations of Al in the IGF (in excess of the compensating Ca concentration), Al ions epitaxially adsorb onto the crystal on the basal side, extending the crystal in this direction.

On the prism side, Al ions adsorb onto the surface with increasing concentration of Al in the IGF. There is a competition for these adsorption sites with the Si and Ca from the IGF, but Al dominate adsorption with increasing Al concentrations.

Figure 7 shows snapshots of thin sections into the plane of the image of the basal and prism interfaces of two IGF compositions. The upper images are from the 221 system, showing poisoning of the basal surface by Ca ions and no growth on that surface, while there is adsorption and extension of the prism side. The lower images show the 141 system, with significant adsorption of Al onto both the prism and basal surfaces, with clearly more growth on the prism side, although the first adsorbed layer on each surface is nearly complete.

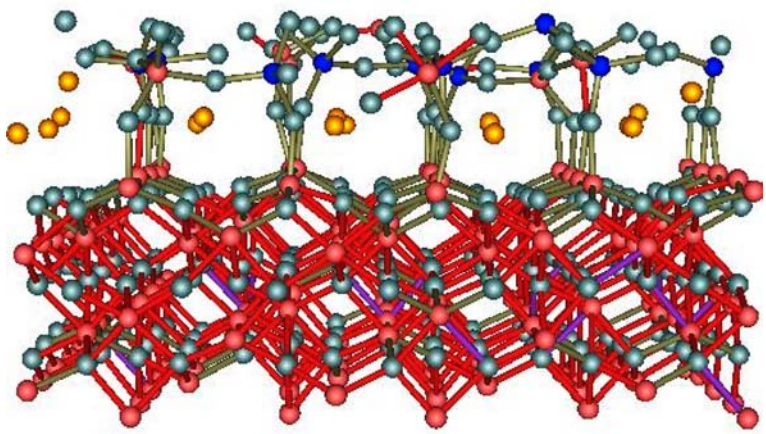

Fig. 6 Sideview of atoms in the basal oriented crystal interfaced with atoms from the IGF. Cage structure forms at the interface, allowing yellow Ca ions adsorption. Red = Al, blue = Si, grey = O, yellow = Ca. Ca–O bonds not drawn

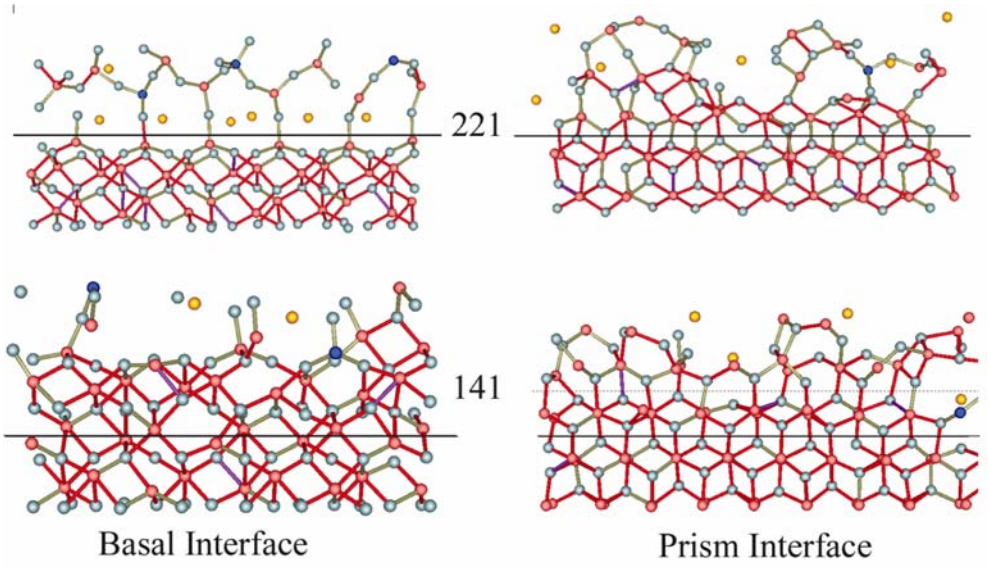

Fig. 7 Snapshots of thin cross-sections of atoms into the plane of the page near the Basal and Prism interfaces of 2 compositions in the simulations. Coordination not accurately depicted in the images because 'bonds' to neighboring atoms not in the image are not drawn. Atoms from the crystal are below the dark solid horizontal line in each image; atoms originally from the IGF are above the dark horizontal line. Atoms between the dashed line and the solid line in 141 Prism image indicates the degree of ordering of the atoms from the IGF that adsorbed onto the crystal surface, forming an extension of the prism oriented crystal. Colors given in Fig.6

The 221 system has a Ca/Al equal to 0.5, which would imply no Ca segregating to the basal surface. However, Ca ions are clearly seen at this interface. The reason for this behavior can be explained by consideration of the concentration of Al in the second adsorbed Al peak, indicated by the dashed arrow in Fig. 3. This second peak of Al is caused by those Al that form at the top of the 'cage' structure shown on the basal side of the 221 system in Fig. 7, providing the second tetrahedrally coordinated Al ion near the Ca ions adsorbed onto the basal surface (the other tetrahedrally coordinated Al ions at the interface are the final layer of Al on the original crystal surface). The concentration of the adsorbed Al in this second Al layer is approximately the same as that for Ca adsorbed onto the basal surfaces for all systems that have a Ca/Al ratio = 0.5 (the 334, 112, and 221 systems). Therefore, the presence of Al in the second adsorbed Al layer enable Ca ions from the IGF interior to segregate to the interface.

Conclusions

The molecular dynamic simulations used here reproduce the appropriate growth anisotropy observed experimentally in alumina without biasing the interatomic potentials to do so. The simulations show the effect of the composition of the intergranular film (IGF) between dissimilarly oriented α-Al_2O_3 crystals on preferential adsorption and growth in the direction of each surface normal. Results show anisotropic adsorption and growth at certain IGF compositions and more isotropic growth at other compositions. Ca ions play the important role of poisoning surface sites on the basal surface, thus inhibiting adsorption of Al onto the surface for growth. The changes in anisotropic and isotropic growth behavior are affected by the Ca/Al ratio in the IGF.

During the kinetic evolution of a system during liquid phase sintering, the composition of the IGF is expected to change in time before reaching an equilibrium composition and thickness. The simulations show that these different compositions affect adsorption of ions from the IGF onto the different crystallographic orientations, subsequently affecting growth and morphology.

Acknowledgement The author acknowledges support from the DOE OBES, Division of Materials Sciences, grant number DE-FG02-00ER45823.

References

1. Kaysser WA, Sprissler M (1987) J Am Ceram Soc 70(5):339
2. Powell-Dogan CA, Heuer AH (1990) J Am Ceram Soc 73(12):3670
3. Powell-Dogan CA, Heur AH, O'Bryan HM (1994) J Am Ceram Soc 77:2593

4. Kleebe H-J (1997) J Ceram Soc Jpn 105:453
5. Kleebe H-J, Cinibulk MK, Cannon RM, Rühle M (1993) J Am Ceram Soc 76(8):1969
6. Pezzotti G, Wakasugi T, Nishida T, Ota R, Kleebe H-J, Ota K (2000) J Non-Cryst Solids 271:79
7. Cinibulk MK, Kleebe H-K, Rühle M (1993) J Am Ceram Soc 76(11):2801
8. Becher PF, Sun EY, Hsueh C-H, Alexander KB, Hwang S-L, Waters SB, Westmoreland CG (1996) Acta Mater 44:3881
9. Brydson R, Twigg PC, Loghran F, Riley FL (2001) J Mater Res 16:652
10. Satet RL, Hoffmann MJ (2004) Key Eng Mat 265–268:775
11. Becher PF, Painter GS, Lance MJ, Ii S, Ikuhara Y (2005) J Am Ceram Soc 88(5):1222
12. Bae SI (1993) J Mat Sci 28:4197
13. Bae J-S, Pyun S-I (1995) J. Alloys Compd 217:52
14. Kwon O-S, Hong S-H, Lee J-H, Chung U-J, Kim D-Y, Hwang NM (2002) Acta Mater 50:4865
15. Altay A, Gulgun MA (2003) J Am Ceram Soc 86(4):623
16. Park CW (2003) J Am Ceram Soc 86(4):603
17. MacLaren I, Cannon RM, Gulgun MA, Ruhle M (2003) J Am Ceram Soc 86(4):650
18. Lange FF (1983) Am Ceram Soc Bull 62(12):1368
19. Tsai RL, Raj R (1980) J Am Ceram Soc 63(9–10):513
20. Raj R (1982) J Geophys Res B 87(7):4731
21. Bae SI, Baik S (1993) J Am Ceram Soc 76(4):1065
22. Ziegler A, Kisielowski C, Hoffmann MJ, Ritchie RO (2003) J Am Ceram Soc 86(10):1777
23. Shibata N, Pennycook SJ, Gosnell TR, Painter GS, Shelton WA, Becher PF (2004) Nature 428:730
24. Winkelman GB, Dwyer C, Marsh C, Hudson TS, Nguyen-Mahn D, Doblinger M, Cockayne DJH (2006) Mater Sci Eng A 422:77
25. Winkelman GB, Dwyer C, Hudson TS, Nguyen-Mahn D, Doblinger M, Satet RL, Hoffmann MJ, Cockayne DJH (2005) Appl. Phys. Lett. 87:061911-1-3
26. Blonski S, Garofalini SH (1996) J Phys Chem 100:2201
27. Blonski S, Garofalini SH (1997) J Am Ceram Soc 80(8):1997
28. Litton DA, Garofalini SH (1999) J Mat Res 14:1418
29. Litton DA, Garofalini SH (2000) J Am Ceram Soc 83(9):2273
30. Marian CM, Gastreich M, Gale JD (2000) Phys Rev B 62:3117
31. Yoshiya M, Tatsumi K, Tanaka I, Adachi H (2002) J Am Ceram Soc 85(1):109
32. Painter GS, Becher PF, Sun EY (2002) J Am Ceram Soc 85(1):65
33. Pezzotti G, Painter GS (2002) J Am Ceram Soc 85(1):91
34. Painter GS, Becher PF, Kleebe H-J, Pezzotti G (2002) Phys Rev B 65:064113-1-11
35. Ching W-Y, Mo S-D, Chen Y (2002) J Am Ceram Soc. 85(1):11
36. Garofalini SH, Zhang S (2003) In Mat. Res. Soc. Symp. Proc., Matls. Res. Soc., Pittsburgh, PA, Boston, p 191
37. Garofalini SH, Luo W (2003) J Am Ceram Soc 86(10):1741
38. Su X, Garofalini SH (2004) J Mat Res 19:3671
39. Su X, Garofalini SH (2004) J Mat Res 19:752
40. Rulis P, Chen J, Ouyang L, Ching W-Y, Su X, Garofalini SH (2005) Phys Rev B 71:235317-1-10
41. Gu H, Pan X, Cannon RM, Rühle M (1998) J Am Ceram Soc 81(12):3125
42. Zhang S, Garofalini SH (2005) J Am Ceram Soc 88(1):202
43. Ravishankar N, Carter CB (2001) Acta Mater 49:1963
44. Blonski S, Garofalini SH (1993) Surf Sci 295:263
45. Delaye J-M, Louis-Achille V, Ghaleb D (1997) J Non-Cryst Sol 210:232
46. Feuston BP, Garofalini SH (1988) J Chem Phys 89(9):5818
47. Litton DA, Garofalini SH (1997) J Non-Cryst Sol 217:250
48. Doblinger M, Cockayne DJH, Meyer RR, Kirkland AI, Nguyen-Mahn D (2004) In 13th European Microscopy Congress, p 59
49. Garofalini SH (2006) Mater. Sci. Eng. A 422:115
50. Batirev IG, Alavi A, Finnis MW, Deutsch T (1999) Phys Rev Lett 82:1510
51. Zirl DM, Garofalini SH (1990) J Am Ceram Soc 73(10):2848
52. Weyl WA, Marboe EC (1964). The constitution of glasses: a dynamic interpretation. J. Wiley, New York